

# Subduction zone forearc serpentinites as incubators for deep microbial life

Oliver Plümper<sup>a,1</sup>, Helen E. King<sup>a</sup>, Thorsten Geisler<sup>b</sup>, Yang Liu<sup>a,c</sup>, Sonja Pabst<sup>d</sup>, Ivan P. Savov<sup>e</sup>, Detlef Rost<sup>f</sup>, and Thomas Zack<sup>g</sup>

<sup>a</sup>Department of Earth Sciences, Utrecht University, 3584 CD Utrecht, The Netherlands; <sup>b</sup>Steinmann Institut für Geologie, Mineralogie und Paläontologie, University of Bonn, 53115 Bonn, Germany; <sup>c</sup>Debye Institute for Nanomaterials Science, Utrecht University, 3584 CC Utrecht, The Netherlands; <sup>d</sup>BHP Billiton Western Australia Iron Ore, Perth, WA 6000, Australia; <sup>e</sup>Institute of Geophysics and Tectonics, School of Earth and Environment, University of Leeds, Leeds LS2 9JT, United Kingdom; <sup>f</sup>Department of Physics, University of Auckland, Auckland 1010, New Zealand; and <sup>g</sup>Department of Earth Sciences, University of Gothenburg, 40530 Gothenburg, Sweden

Edited by Norman H. Sleep, Stanford University, Stanford, CA, and approved March 10, 2017 (received for review July 27, 2016)

**Serpentinization-fueled systems in the cool, hydrated forearc mantle of subduction zones may provide an environment that supports deep chemolithoautotrophic life. Here, we examine serpentinite clasts expelled from mud volcanoes above the Izu–Bonin–Mariana subduction zone forearc (Pacific Ocean) that contain complex organic matter and nanosized Ni–Fe alloys. Using time-of-flight secondary ion mass spectrometry and Raman spectroscopy, we determined that the organic matter consists of a mixture of aliphatic and aromatic compounds and functional groups such as amides. Although an abiotic or subduction slab-derived fluid origin cannot be excluded, the similarities between the molecular signatures identified in the clasts and those of bacteria-derived biopolymers from other serpentinizing systems hint at the possibility of deep microbial life within the forearc. To test this hypothesis, we coupled the currently known temperature limit for life, 122 °C, with a heat conduction model that predicts a potential depth limit for life within the forearc at ~10,000 m below the seafloor. This is deeper than the 122 °C isotherm in known oceanic serpentinizing regions and an order of magnitude deeper than the downhole temperature at the serpentinized Atlantis Massif oceanic core complex, Mid-Atlantic Ridge. We suggest that the organic-rich serpentinites may be indicators for microbial life deep within or below the mud volcano. Thus, the hydrated forearc mantle may represent one of Earth's largest hidden microbial ecosystems. These types of protected ecosystems may have allowed the deep biosphere to thrive, despite violent phases during Earth's history such as the late heavy bombardment and global mass extinctions.**

deep biosphere | serpentinization | subduction zone | forearc

Microbial life may be sustained within the lithosphere by mineral-mediated chemical reactions that provide usable energy resources (1). For example, redox-coupled reactions during serpentinization, the formation of serpentine [(Mg,Fe)<sub>3</sub>Si<sub>2</sub>O<sub>5</sub>(OH)<sub>4</sub>] through mantle olivine [(Mg,Fe)<sub>2</sub>SiO<sub>4</sub>] hydration, generate substantial amounts of H<sub>2</sub> (2). Although serpentinization leads to extreme pH conditions and limited nutrient and electron acceptor availability (1), microgenomic studies of serpentinization-fueled hydrothermal deep-sea vents and continental fluid seeps show evidence for microbial H<sub>2</sub> and CH<sub>4</sub> utilization (1, 3–5). Furthermore, micrometer-sized organic matter has been detected in dredged seafloor serpentinites (6) and in subseafloor mixing zones between seawater and serpentinization-derived fluid (7). The former study suggests that serpentinization-fueled microbial communities may use solid electron acceptors, particularly ferric iron from magnetite (Fe<sub>2</sub>O<sub>3</sub>) or other Fe(III)-bearing minerals, such as andradite garnets [Ca<sub>3</sub>Fe(III)<sub>2</sub>Si<sub>3</sub>O<sub>12</sub>] (8). However, the architecture of potentially habitable domains within Earth's hydrated mantle rocks remains largely unknown. Understanding the possible relationship between mineral reactions and biological activity requires identification of in situ signatures of the deep biosphere that allow us to plunge beneath the Earth's surface to assess its extent and how mineral reactions may support or even form life. Serpentine clasts recovered from the

South Chamorro mud volcano [13°47'N, 146°00'E; Ocean Drilling Program (ODP) Leg 195] above the Izu–Bonin–Mariana (IBM) subduction zone (9) (Fig. 1) can potentially provide just such a window into the deep biosphere. The mud volcanoes source their serpentine from >20-km depth via deep-reaching forearc faults, where serpentinite gouges mix with slab-derived fluids before buoyantly rising toward the seafloor (10).

## IBM Subduction Zone and Serpentine Mud Volcanism

The IBM subduction zone is a convergent plate margin ranging over ~2,800 km from near Tokyo (Japan) to south of Guam (Mariana Islands; Fig. 1). The IBM is located along the eastern margin of the Philippine Sea Plate in the Western Pacific Ocean and formed due to the subduction of the Pacific Plate under the Philippine Sea Plate (11). The southern boundary is marked by the intersection of the IBM trench with the Palau–Kyushu Ridge at 11°N. The northern boundary is at 35°20'N close to southern Honshu, Japan (12). The eastern boundary extends along a deep-sea trench and ranges in depth from 3 km at the Ogasawara Plateau (trench entrance) to ~11-km depth within the Challenger Deep—the deepest site in the world. The Mariana forearc is pervasively faulted by tectonic activity and only minor sediment accretion occurs along the margin (9, 13). As the Pacific Plate descends, oceanic upper mantle, oceanic crust, overlying sediment, and water are transported into the forearc mantle. Some of this material is transferred from the subducting slab into the overlying mantle and oceanic plate, where large quantities of fluids rise through faults and fractures, carrying dissolved

## Significance

**We document organic matter encapsulated in rock clasts from a oceanic serpentinite mud volcano above the Izu–Bonin–Mariana subduction zone (Pacific Ocean). Although we cannot pinpoint the exact origin of the organic matter, chemical analysis of the constituents resembles molecular signatures that could be produced by microbial life deep within or below the mud volcano. Considering the known temperature limit for life, 122 °C, and the subduction zone forearc geotherm where such mud volcanoes are located, we estimate that life could exist as deep as ~10,000 m below the seafloor. This is considerably deeper than other active serpentinizing regions such as midocean ridges and could have provided sheltered ecosystems for life to survive the more violent phases of Earth's history.**

Author contributions: O.P. designed research; O.P., H.E.K., T.G., Y.L., S.P., I.P.S., D.R., and T.Z. performed research; T.G., Y.L., D.R., and T.Z. contributed analytic tools; O.P., H.E.K., T.G., Y.L., S.P., D.R., and T.Z. analyzed data; and O.P., H.E.K., and T.Z. wrote the paper.

The authors declare no conflict of interest.

This article is a PNAS Direct Submission.

Freely available online through the PNAS open access option.

<sup>1</sup>To whom correspondence should be addressed. Email: o.plumper@uu.nl.

This article contains supporting information online at [www.pnas.org/lookup/suppl/doi:10.1073/pnas.1612147114/-DCSupplemental](http://www.pnas.org/lookup/suppl/doi:10.1073/pnas.1612147114/-DCSupplemental).

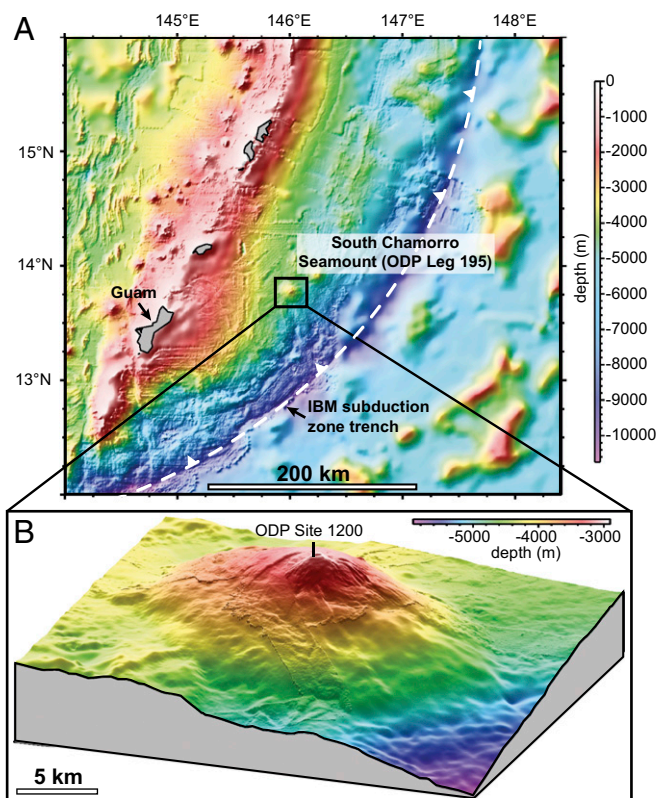


**Fig. 1.** Location of the South Chamorro serpentinite mud volcano and the Izu–Bonin–Mariana (IBM) subduction zone (modified from ref. 11). (A) Bathymetry map of the Mariana arc-basin system displaying the location of the South Chamorro Seamount (Leg 195) in relation to the volcanic islands such as Guam. Approximately 50 km south of the seamount the water depth exceeds 8 km highlighting the trench of the IBM subduction zone that runs approximately north to southwest. (B) Three-dimensional view of the South Chamorro Seamount, depicting the location of ODP Site 1200. The subducting Pacific slab beneath the serpentinite mud volcano is in ~20-km depth.

constituents from the subducting slab. These fluids can either vent as cold springs onto the seafloor (14) or hydrate and serpentinize the mantle wedge. The latter is supported by deep-sea drilling and geophysical measurements showing that at least part of the Mariana forearc mantle wedge is hydrated (15, 16). Within the deep-reaching forearc faults, serpentinite fault gouges mix with the rising slab-derived fluids. This mud–rock mixture buoyantly rises in conduits along fault planes until it extrudes onto the seafloor to form various kilometer-scale seamounts, that is, mud volcanoes, predominantly composed of serpentinite, situated on the outer forearc of the Mariana margin (e.g., ref. 17) (Fig. 1B). The mud volcanoes are located in a trench-parallel zone ~30–100 km arcward of the trench axis and reach up to 50 km in diameter and over 2 km in height (17, 18). Unconsolidated flows of clay- to silt-sized serpentinite mud enclose up to boulder-sized rock clasts of variably serpentinized mantle peridotite and subordinately blueschist-facies fragments (18). The samples studied here are recovered from drill cores taken from the South Chamorro serpentinite mud volcano (13°47'N, 146°00'E; Fig. 1B) drilled during ODP Leg 195 (19). The seamount is a partly collapsed, roughly conical structure ~2-km high and ~20-km wide with active serpentine/blueschist mud volcanism. The subducting slab beneath the serpentinite mud volcano is at ~20-km depth (14, 18).

### Serpentinite Clasts from the South Chamorro Mud Volcano

We studied 46 clasts recovered at depths of 14.80 (1200E-004-02WR-130-140), 28.70 (1200E-007H-02WR-130-140), and 110.07 m below seafloor (mbsf) (1200A-013R-02W-40877). All clasts show a

serpentinite mesh texture, where lizardite veins assemble as a mesh framework encompassing central mesh cores (Fig. 2A and B). Mesh cores are typically composed of chrysotile, or occasionally a mixture of lizardite and chrysotile. In some instances, lizardite fully overgrows the mesh core region (*SI Raman Spectroscopy*). Time-of-flight secondary ion mass spectrometry (ToF-SIMS) detected aliphatic ion species and ionic units within the mesh cores from a clast retrieved from 14.80 mbsf (Fig. 2C–E). These ion clusters have previously been used as indicators for the presence of the amino acids methionine,  $C_5H_{11}NO_2S$ , and threonine,  $C_4H_9NO_3$  (20), but could arise from other organic molecules with a similar mass. Confocal micro-Raman spectroscopy corroborates the ToF-SIMS findings showing the presence of amide functional groups within the organic material as well as aliphatic and aromatic functional groups (Fig. 2F). Hyperspectral Raman imaging (*Methods* and *SI Raman Spectroscopy*) reveals the almost exclusive accumulation of such structural components of organic compounds within the mesh cores (Fig. 2G), in agreement with the ToF-SIMS results (Fig. 2C–E). Clasts retrieved from greater depth within the ODP Leg 195 core (110.07 mbsf) display nearly identical Raman spectra indicative of organic material (Fig. 2F). However, the additional N(C–C) stretching mode is absent, likely reflecting varying degrees of maturity.

Brucite and magnetite associated with lizardite within the clasts constrains the serpentinization temperature to below 300 °C (21). We also identified nanosized (50–350 nm) awaruite ( $Ni_{2-3}Fe$ ) grains embedded within and in the vicinity of the mesh cores (Fig. 3A–C; *SI Opaque Mineral Grain Analysis*). The ToF-SIMS measurements further reveal elevated concentrations of various redox active metal ions (Mn, Ni, Cr, Fe; Fig. 3D) encompassing the organic-rich mesh cores shown in Fig. 2. Nanotomography, acquired by focused ion beam scanning electron microscopy (FIB-SEM), shows that the mesh cores are areas of elevated porosity (Fig. 4A). Based on the segmented nanotomography volume

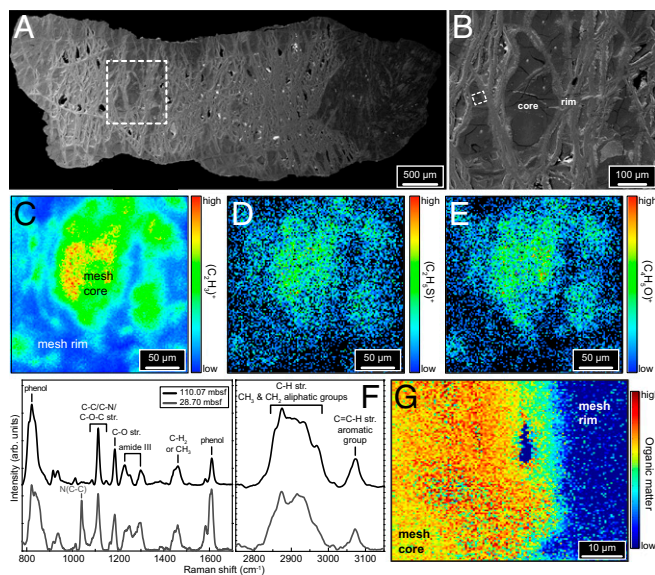


**Fig. 2.** Organic matter within mesh-textured serpentinite clasts. (A and B) Backscattered electron images of a clast cross-section from 28.70 mbsf (1200E-007H-02WR-130-140). Dashed square in A depicts magnified area in B. (C–E) ToF-SIMS maps of a core–rim region in a clast from 14.80 mbsf (1200E-004-02WR-130-140) showing that the mesh core is enriched in  $(C_2H_5)^+$ ,  $(C_2H_5S)^+$ , and  $(C_4H_5O)^+$ . (F) Raman spectra obtained from an area in B (dashed rectangle) and a clast from 110.07 mbsf (1200A-013R-02W-40877) show organic molecules. (G) Hyperspectral Raman imaging (dashed rectangle in B) reveals organic material in the mesh cores and no organics within the rims, consistent with C–E.

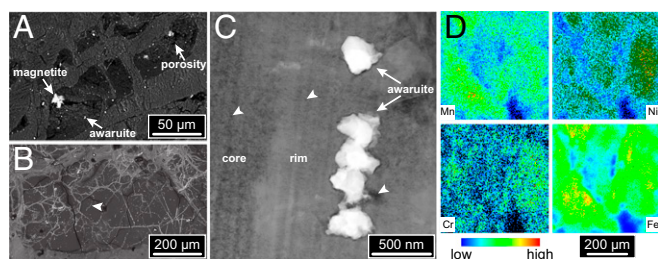


**Fig. 3.** Distribution of redox-sensitive transition metals in a mesh-textured serpentinite clast. (A and B) Backscattered electron images and (C) high-angle annular dark-field scanning transmission electron microscope (HAADF-STEM) image showing nanosized awaruite grains in the vicinity of mesh cores (bright spots in B; arrowhead). Mesopores (arrowhead in C) surrounding awaruite grains and extending across the rim–core interface could potentially allow gaseous exchange between nanograin surfaces and serpentinite mesh cores. A and B are images from samples retrieved from 14.80 and 110.07 mbsf, respectively. ToF-SIMS maps in D show elevated concentrations of redox-active metal ions encompassing the organic-rich mesh core shown in Fig. 2C.

shown in Fig. 4A, the visible median pore size is  $\sim 25$  nm. However, considerably larger pore structures, exceeding several micrometers, can be found in other mesh cores (Fig. 3A). Pore formation is likely the result of several factors such as imperfect packing of randomly orientated serpentinite grains as typically observed in serpentinite mesh cores (22), chrysotile nanopores (22, 23), prolonged exposure to upwelling subduction zone fluids inducing mineral dissolution, and/or decompression cracking during upward migration along faults or within the mud volcano conduit. Mesh rims are typically characterized by fewer, micrometer-sized pores (Fig. 4B and C) as well as mesopores (i.e., 2–50 nm) in the vicinity of mesh cores and around awaruite grain clusters (Fig. 3C). The anisotropic pore alignment (Fig. 4A) and complex pore contrast (Fig. 4B) indicate that the mesh cores contain a partially connected pore network. The intricate relationship between the serpentinite and organic matter (Fig. 2), however, suggests that the detected pore sizes are substantially underestimated as the organic material within the pores obscures the true pore size that is likely orders of magnitude larger.

Although we cannot unambiguously assign the source of the organic matter, several steps can be taken toward better constraining its potential origin. Upon contact with seawater, the high pH ( $\sim 12.6$ ) pore fluids with high alkalinity (100 mmol/kg) within the muds found at the South Chamorro mud volcano should trigger immediate carbonate precipitation (24). The absence of any carbonate within the clast-bearing mud layers from 28.70 and 110.07 mbsf thus suggests that, although the clasts were erupted onto the seafloor, they were never exposed to seawater and thus seawater-derived organic matter. Additionally, organic matter was only identified in the internal regions of the serpentinite clasts after cross-sectional opening of the clasts (Fig. 2A). Therefore, it seems unlikely that the organic matter was introduced during shipboard sampling, storage, or sample preparation (Methods). Other potential sources would be organic matter derived from subducted pelagic sediments or in situ production within the forearc system via abiotic or biological processes. Isotope studies suggest influx of fluids derived from a mixture of subducted pelagic sediments and altered oceanic crust into the forearc mantle facilitating serpentinitization (25). However, their sources remain controversial (26–28), and the nature of the organic material that is potentially carried with these fluids is largely unknown. Abiotic routes have been demonstrated to produce hydrocarbons and amino acids under hydrothermal conditions akin to serpentinitization (29), but it is unclear whether these processes can produce the organic complexity observed in

the serpentinite clasts. Intriguingly, similar Raman spectra to those reported here have been documented in other serpentinites and correlate with spectra taken from bacteria (6) and the presence of bacterial lipid biomarkers (7). Moreover, the acquired Raman spectra (Fig. 2F) show bands in similar positions to those attributed to functional modes typically found in bacteria-derived biopolymers, including proteins, lipids, and nucleic acids (30, 31), indicating that the organics may have a biological source.

### Depth Limit for Microbial Life Within Subduction Zone Forearc

To test whether microbial life is a feasible source of the organic matter observed, we need to establish an estimate for the depth limit for life within the Mariana forearc. As microbial organisms can survive temperatures as high as 122 °C (32) and pressures into the gigapascal range (33), we estimated the potential depth limit for microbial life in this region using a one-dimensional steady-state heat conduction model (34) (*SI Estimation of the Maximum Depth for the Current Temperature Limit for Life*). In this calculation, heat is transferred in one direction without consideration of minor advective heat flow through the ascending mud or heat generated through the exothermic serpentinitization reaction. Both of these processes are expected to only play a minor role. Particularly heat through serpentinitization has been shown to be nearly negligible (35). Assuming no variations in temperature or heat flow, the basic equation of conductive heat transfer theory is a statement of conservation of energy and can be written as follows:

$$T = T_0 + \frac{q_0}{k} y - \frac{\rho H}{2k} y^2, \quad [1]$$

where  $T$  and  $T_0$  are the temperature at depth and at the ocean floor,  $y$  is the depth in meters below seafloor,  $q_0$  is the surface heat flow ( $0.03 \text{ W}\cdot\text{m}^{-2}$ ),  $k$  is the thermal rock conductivity ( $2.9 \text{ W}\cdot\text{m}^{-1}\cdot\text{K}^{-1}$ ),  $\rho$  is the density ( $2,900 \text{ kg}\cdot\text{m}^{-3}$ , partially serpentinitized peridotite), and  $H$  is the current mean mantle heat generation rate due to radioactive decay ( $7.42 \times 10^{-12} \text{ W}\cdot\text{kg}^{-1}$ ) (34). At relatively shallow forearc depths,  $H$  will only play a minor role. Rearranging the equation above to solve for  $y$  at a given temperature (i.e., the known temperature limit for life at 122 °C) results in the following:

$$y_{\pm} = \frac{q_0 \pm \sqrt{2T_0 H k \rho - 2H k \rho T + q_0^2}}{H \rho}, \quad [2]$$

where  $y_{\pm}$  is a nonphysical solution and thus disregarded. Surface heat flow values of the Mariana forearc were taken from measurements acquired during the Deep Sea Drilling Project Leg 60

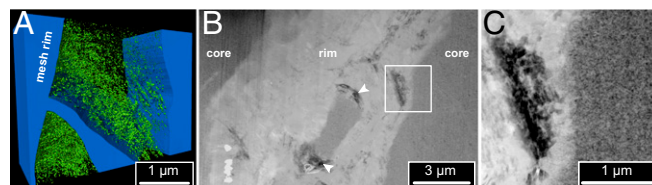


**Fig. 4.** Porosity within an organic-bearing, mesh-textured serpentinite clast. (A) Three-dimensional visualization of a FIB-SEM nanotomography volume ( $14.8 \times 11.05 \times 5.3 \mu\text{m}$ ) showing that mesh cores consist of an extensive network of aligned mesopores (green), whereas the rims (blue) are mainly characterized by individual micrometer-sized pores (arrowheads) as shown in HAADF-STEM image (B). (C) HAADF-STEM image of the interface between the mesh rim and the core (white rectangle in B). Note the pore size difference between mesh rim and core and the complex contrast in the core indicating nanoscale pore connectivity.

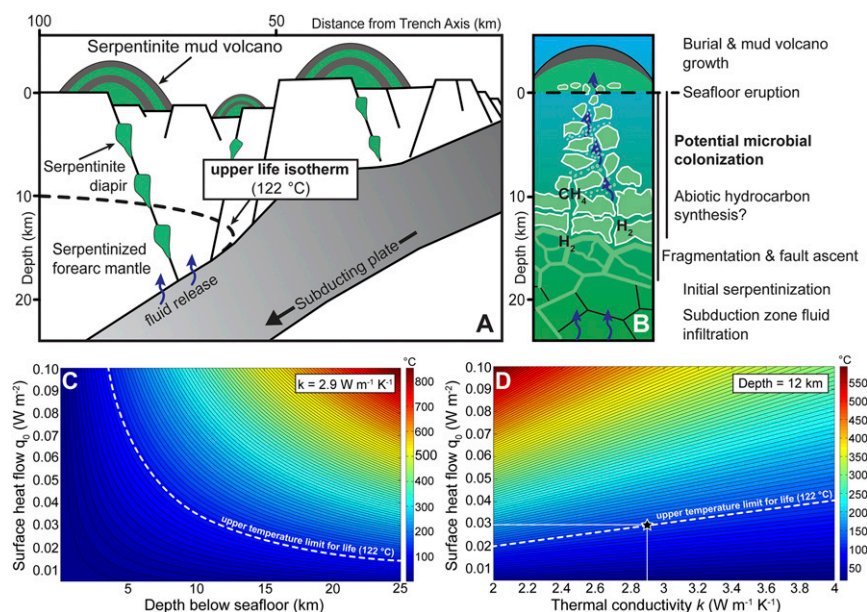


**Fig. 5.** Conceptual model of a deep biosphere environment within the IBM subduction zone forearc with limit for serpentinization-fueled microbial life estimated at 10,000 mbsf based on the known upper temperature limit for life (122 °C) (34) and our heat conduction model. **A** shows a cross-sectional sketch of the IBM forearc. Fluid release from the subducting plate results in partial forearc mantle serpentinization. Tectonic activity causes mud–rock mixture to rise buoyantly in conduits along fault planes until it protrudes onto the seafloor to form massive serpentinite mud volcanoes (up to 50-km diameter and >2 km above the surrounding seafloor). The sketch in **B** displays a conceptual serpentinization evolution model and the depth range for possible subsurface microbial colonization. **C** and **D** show results of the one-dimensional heat conduction model (*SI Estimation of the Maximum Depth for the Current Temperature Limit for Life*), where **C** shows the maximum depth as a function of surface heat flow at constant thermal conductivity (partially serpentinized peridotite) below which microbial life is theoretically possible. **D** displays the influence of surface heat flow and thermal conductivity, at an average depth of 12,000 mbsf, on the upper temperature limit for life.

(36). Thermal conductivity values of serpentinites are based on measurements taken during ODP 209 (37) and an average value of  $2.9 \text{ W} \cdot \text{m}^{-1} \cdot \text{K}^{-1}$  is used. Using these values, the maximum depth for the 122 °C isotherm varies between ~8,000 and 15,000 mbsf (Fig. 5C). These depth estimates are based on surface heat flow values of  $0.03\text{--}0.04 \text{ W} \cdot \text{m}^{-2}$  that agree with the observed depression of isotherms in most forearc mantle wedges, even those of relatively hot origin such as the Cascadia subduction zone (38, 39). Moreover, our thermal calculations are in agreement with more complex geodynamic models (40, 41), confirming that the 122 °C isotherm is reached at ~10,000 mbsf in forearcs. Hence, current serpentinization-fueled microbial life within subduction zone forearcs could be supported down to these depths and corresponding pressure (~0.34 GPa; Fig. 5). In contrast, habitable zones in the vicinity of oceanic spreading centers are limited to the first hundred meters to few kilometers below the seafloor. The exact location of the 122 °C isotherm will likely vary in depth at and around the spreading center as a result of the ridge architecture, heat flux, and hydrothermal circulation (42, 43). The downhole temperature within the International Ocean Drilling Program (IODP) Hole U1309D at Atlantis Massif oceanic core complex (Mid-Atlantic Ridge) places the 122 °C upper temperature limit for microbial life at ~1,000 mbsf (44). This is one order of magnitude less than compared with our estimated limit of life in the Mariana subduction zone forearc. As the serpentinite mud originates directly from the forearc mantle wedge (>20-km depth), the model indicates the potential for a biosphere deep within the forearc. This makes the Mariana serpentinite clasts a natural laboratory of prime interest when searching for habitable zones of life deep within the lithosphere.

### Sustaining Microbial Life Within Subduction Zone Forearcs

To sustain deep microbial life within a solid rock framework requires energy resources that can either migrate or be produced

close to areas suitable for colonization. There is little to no chemical benefit for microbes to interact directly with serpentine minerals; thus, other life-supporting energy-generating pathways need to be present. Microgenomic studies show evidence for microbial  $\text{H}_2$  and  $\text{CH}_4$  utilization in serpentinizing systems with known microbial colonization. Indeed, several studies (e.g., ref. 5) indicate that *Archaea* found up to 20 mbsf within the South Chamorro mud volcano are fueled by deeply derived  $\text{CH}_4$ -enriched fluids. Experiments suggest that  $\text{H}_2$  produced during low-temperature serpentinization (<200 °C) (45) could react with a carbon source to form  $\text{CH}_4$  on catalytic mineral surfaces. Investigations of naturally occurring abiogenic  $\text{CH}_4$  indicate that abiotic hydrocarbon synthesis can potentially take place at temperatures as low as ~120 °C (46). However, there are contrasting experimental results concerning the formation and synthesis kinetics of  $\text{CH}_4$  production at (very) low temperatures (47–49). In hydrothermal experiments, awaruite has been identified as a possible  $\text{CH}_4$  production catalyst (50). The awaruite grains observed here are nanosized (Fig. 3C) and, therefore, have a high surface area-to-volume ratio, which should enhance their catalytic activity (51). Thus, nanosized alloys could have facilitated  $\text{CH}_4$  production over geologically relevant timescales below the upper temperature limit for life (122 °C). In near-surface serpentinizing systems, hydrothermal fluids can mix with, for example, seawater, resulting in disequilibria that may provide the energy and substrates needed to support chemolithoautotrophic life (7). In contrast, a slowly ascending serpentinite mud along deep-reaching forearc faults may allow the system to remain much closer to equilibrium, regulating the activities of  $\text{H}_2$ ,  $\text{CH}_4$ ,  $\text{CO}_2$ , and the Fe(II)/Fe(III) ratio in the solids and fluids limiting energy sources. Nielsen et al. (25), however, documented the occurrence of rodingite within the Mariana serpentinite mud volcanoes derived from in situ alteration within the forearc mantle. These rocks suggest hydrothermal interactions between

mafic and ultramafic units and together with simultaneous serpentinization may be the source of fluids that can produce disequilibrium environments.

An additional source of externally derived fluids could come directly from the subducting slab and would thus be in disequilibrium with the overriding forearc wedge. These fluids are most likely different in composition compared with serpentinizing systems at midocean ridges or passive margins. Kelemen and Manning (52) recently reevaluated the global carbon flux through subduction zones and estimated that several million tons of carbon per year could be released from subducting slabs into the overriding forearc wedge. Therefore, these fluids could provide the carbon source needed for abiotic hydrocarbon synthesis or even directly contribute organic molecules to the forearc and thus the serpentinite clasts. If the organic matter reported here was sourced from the subduction slab alone, we would expect the same level of maturation and thus evidence for the same functional groups. However, we observe the absence of specific Raman bands [N(C–C)] in clasts from different depths (Fig. 2*F*). Various studies have shown that subduction zone dehydration reactions across a range of temperatures (200–600 °C) and pressures release nitrogen that is able to enter the overriding forearc directly or travel with the expelled fluids upward through the subduction zone channel (53–55). Moreover, recent thermodynamic calculations of the nitrogen speciation in aqueous fluids under upper mantle conditions suggest that the oxidized mantle wedge of subduction zones favors nitrogen over ammonium (NH<sub>4</sub><sup>+</sup>), promoting outgassing rather than mineral trapping of nitrogen (56). Thus, the actions of mud volcanoes as conduits for slab-derived fluids may provide missing resources that would otherwise be limiting factors for life in the forearc mantle or contribute nitrogen to the abiotic synthesis of more complex organic compounds. To rigorously evaluate the energy sources for microbial life within the subduction zone forearc, better constraints are needed for the fluid influxes from the subduction zone and how these slab-derived fluids interact with the forearc. Increasing sophisticated fluid speciation models coupled to fluid–rock interaction simulations and experiments at high pressures and temperatures (56, 57) will provide critical insights into this problem.

## Implications

Although the origin of the organic matter cannot be unequivocally identified, we suggest, based on the similarities with molecular signatures of bacteria-derived biopolymers, that the organic matter may represent remnants of microbial life within or even below the mud volcanoes. Our simple model supports this hypothesis, showing that the temperature window for life could extend deep into the forearc. Hence, the identification of complex organic matter recovered from depths of up to 110.07 mbsf may be evidence for life in an oceanic serpentinite-hosted rock formation from depths likely far exceeding the drill core depth, where serpentinite-supported life has not yet been documented. Thus far, evidence for microbial communities within the Mariana mud volcanoes has only been indirectly detected in fluid samples no deeper than 20 mbsf (5, 24). There are a variety of examples indicating that microbial life can colonize shallow serpentinization-fueled environments and use abiogenically produced H<sub>2</sub> and CH<sub>4</sub> (1, 3–5), but microbial life within the deep subsurface, for example, deep within the Mariana forearc, with no connection to the Earth's surface, may have little resemblance with presently known serpentinization-fueled ecosystems.

In any case, if life is present in the subduction zone forearc, it has far-reaching implications as recent studies suggest that environments resembling those both within and below the Mariana serpentinite mud volcanoes were already present on the early Earth (58, 59). Thus, even if modern-type subduction was not fully established in the Hadean and Archean, Mariana forearc-like deep subsurface environments may have allowed early forms

of life to thrive, despite violent phases such as the so-called Late Heavy Bombardment, a period of intensive meteorite bombardment around 3.9 Ga (60). Even if only a small amount of the global forearc mantle hosts microbial life, fluctuations in the total subduction zone length (61) could have significant consequences for the deep carbon budget. During these fluctuations, fluid flow through subduction zone forearc regions, visible in the form of serpentinite mud volcanism, are a crucial connection between the deep biosphere and surface world, influencing geochemical fluxes throughout Earth's history. Only if we keep exploring the windows into the deep subsurface, such as the serpentinite clasts presented here, will we be able to establish a full budget of Earth's deep carbon and the potential for a subsurface biosphere.

## Methods

**Sample Preparation.** Drilling during ODP Leg 195 was executed with the support of inorganic drilling mud (mainly sepiolite) and seawater. Immediately after the core was recovered, a 6-in. length of whole-round core was cut and refrigerated. Samples (diameter, 4.25 cm) were removed from the whole-round core using a piston core sampler. These subcores were loaded into a Manheim squeezer for the analysis of physical properties (62). The applied axial pressure (6.3 MPa) under drained conditions is insufficient to cause pore collapse within individual clasts. From the “squeeze cakes,” 1/4 rounds were extracted for further onshore analysis and stored in a nonsterile fashion. Serpentinite clasts, hundreds of micrometers to a few millimeters in size, were extracted from these mud-pellets rounds by dissolution in distilled water and hand picking under a binocular microscope. Clasts were mounted in 1-in. round sections using epoxy resin and polished to expose the internal structures. The samples were not subjected to a vacuum impregnation step to avoid the penetration of epoxy into open spaces. For Raman spectroscopic details of the epoxy, see *SI Raman Spectroscopy*. To avoid laboratory contamination before microstructural and microchemical investigations, the samples were treated with 5% sodium hypochlorite and repolished using a diamond paste and concentrated ethanol to expose fresh sample surfaces. Subsequently, samples were again treated with 5% sodium hypochlorite.

**ToF-SIMS.** Element distribution maps were obtained using an ION-TOF ToF-SIMS IV instrument at the Smithsonian Institution's National Museum of Natural History (Washington, DC). The 25-kV 69Ga<sup>+</sup> primary ion column was operated in a low-current bunched mode with a cycle time of 45 μs, allowing for a mass resolution (full width half-maximum) of 4,600 at nominal mass 61 u (C<sub>2</sub>H<sub>5</sub>S)<sup>+</sup>. To remove surface contamination, an area four times larger than the analytical field of view was sputter-cleaned with a 3-keV Ar<sup>+</sup> ion beam before the actual measurement.

**FIB-SEM and Transmission Electron Microscopy.** Scanning electron microscopy (SEM) investigations on Pt-coated specimens were carried out in a JEOL JCM-6000. A FEI Nova Nanolab FIB-SEM was used to acquire nanotomography volumes (voxel size, 2.5 × 2.5 × 10 nm) and to extract electron transparent foils for transmission electron microscopy (TEM). FIB-SEM nanotomography was carried out at an acceleration voltage of 2 kV and a beam current of 0.21 nA. The nanotomography volumes were visualized and analyzed using Avizo 9. TEM investigations were executed in a FEI Tecnai 20F operated at 200 kV equipped with a high-angle annular dark field (HAADF) detector and an energy-dispersive X-ray (EDX) spectroscopy system.

**Raman Spectroscopy.** Raman spectra of organic matter were collected using a near-infrared (784/785 nm) laser of a Horiba Scientific LabRam HR800 and a Kaiser HoloLab Series 5000. Hyperspectral Raman mapping of the organic matter distribution was executed with a lateral resolution of ~1 μm and a spectral resolution of 2.3 cm<sup>-1</sup>. Analysis of the “fingerprinting” serpentine OH bands was performed using a 532-nm laser of a WITec alpha 300R. Further information about instrument settings and Raman spectra analysis is found in *SI Raman Spectroscopy*.

**ACKNOWLEDGMENTS.** We thank T. Ludwig for discussion. O.P. was supported by Netherlands Organization for Scientific Research Veni Grant 863.13.006, H.E.K. by the European Union Fellowship PIOF-GA-2012-328731, T.Z. by the German Science Foundation (ZA285/5), and Y.L. by the Utrecht University Sustainability Program. For I.P.S., Ocean Drilling Program (ODP) Leg 195 participation and post-cruise research were funded by Joint Oceanographic Institutes/US Science Advisory Committee (Schlanger Fellowship) and the UK International Ocean Discovery Program (IODP) Program via the Natural Environment Research Council (NE/M007782/1).

- Schrenk MO, Brazelton WJ, Lang SQ (2013) Serpentinization, carbon, and deep life. *Rev Mineral Geochem* 75:575–606.
- McCullom TM, Bach W (2009) Thermodynamic constraints on hydrogen generation during serpentinization of ultramafic rocks. *Geochim Cosmochim Acta* 73:856–875.
- Ohara Y, et al. (2012) A serpentinite-hosted ecosystem in the Southern Mariana Forearc. *Proc Natl Acad Sci USA* 109:2831–2835.
- Brazelton WJ, Nelson B, Schrenk MO (2012) Metagenomic evidence for H<sub>2</sub> oxidation and H<sub>2</sub> production by serpentinite-hosted subsurface microbial communities. *Front Microbiol* 2:268.
- Curtis AC, Wheat CG, Fryer P, Moyer CL (2013) Mariana forearc serpentinite mud volcanoes harbor novel communities of extremophilic archaea. *Geomicrobiol J* 30:430–441.
- Menez B, Pasini V, Brunelli D (2012) Life in the hydrated suboceanic mantle. *Nat Geosci* 5:133–137.
- Klein F, et al. (2015) Fluid mixing and the deep biosphere of a fossil Lost City-type hydrothermal system at the Iberia Margin. *Proc Natl Acad Sci USA* 112:12036–12041.
- Plümpner O, Beinlich A, Bach W, Janots E, Austrheim H (2014) Garnets within geode-like serpentinite veins: Implications for element transport, hydrogen production and life-supporting environment formation. *Geochim Cosmochim Acta* 141:454–471.
- Salisbury MH, Shinohara M, Richter C (2002) *Proceedings of the Ocean Drilling Program, Initial Reports, 195* (Ocean Drilling Program, College Station, TX).
- Fryer P, Wheat CG, Mottl MJ (1999) Mariana blueschist mud volcanism: Implications for conditions within the subduction zone. *Geology* 27:103–106.
- Savov IP, Ryan JG, D'Antonio M, Fryer P (2007) Shallow slab fluid release across and along the Mariana arc-basin system: Insights from geochemistry of serpentinized peridotites from the Mariana fore arc. *J Geophys Res Solid Earth* 112:B09205.
- Stern RJ, Fouch MJ, Klemperer SL (2003) An overview of the Izu-Bonin-Mariana subduction factory. *Inside the Subduction Factory*, Geophysical Monograph, ed Eiler J (American Geophysical Union, Washington, DC), Vol 138, pp 175–222.
- Horine RL, Moore GF, Taylor B (1990) Structure of the outer Izu-Bonin forearc from seismic-reflection profiling and gravity modeling. *Proceedings of the Ocean Drilling Program, Initial Reports*, eds Fryer P, et al. (Ocean Drilling Program, College Station, TX), pp 81–94.
- Mottl MJ, Wheat CG, Fryer P, Gharib J, Martin JB (2004) Chemistry of springs across the Mariana forearc shows progressive devolatilization of the subducting plate. *Geochim Cosmochim Acta* 68:4915–4933.
- Bostock MG, Hyndman RD, Rondenay S, Peacock SM (2002) An inverted continental Moho and serpentinization of the forearc mantle. *Nature* 417:536–538.
- Kamimura A, et al. (2002) Crustal structure study at the Izu-Bonin subduction zone around 31 °N: Implications of serpentinized materials along the subduction plate boundary. *Phys Earth Planet Inter* 132:105–129.
- Fryer P, Pearce J, Stokking L (1992) A synthesis of Leg 125 drilling of serpentine seamounts on the Mariana and Izu-Bonin forearcs. *Proceedings of the Ocean Drilling Program, Scientific Results* (Ocean Drilling Program, College Station, TX), pp 593–614.
- Fryer P, Lockwood JP, Becker N, Phipps S, Todd CS (2000) Significance of serpentinite mud volcanism in convergent margins. *Geol Soc Am* 349:35–51.
- Fryer P, Salisbury M (2006) Leg 195 synthesis: Site 1200-Serpentinite seamounts of the Izu-Bonin/Mariana convergent plate margin (ODP Leg 125 and 195 drilling results). *Proceedings of the Ocean Drilling Program, Scientific Results* (Ocean Drilling Program, College Station, TX), pp 1–30.
- Wagner MS, McArthur SL, Shen M, Horbett TA, Castner DG (2002) Limits of detection for time of flight secondary ion mass spectrometry (ToF-SIMS) and X-ray photoelectron spectroscopy (XPS): Detection of low amounts of adsorbed protein. *J Biomater Sci Polym Ed* 13:407–428.
- Evans BW (2010) Lizardite versus antigorite serpentinite: Magnetite, hydrogen, and life. *Geology* 38:879–882.
- Viti C, Mellini M (1998) Mesh textures and bastites in the Elba retrograde serpentinites. *Eur J Mineral* 10:1341–1359.
- Dódony I, Buseck PR (2004) Serpentine close-up and intimate: An HRTEM view. *Int Geol Rev* 46:507–527.
- Mottl MJ, Komor SC, Fryer P, Moyer CL (2003) Deep-slab fuel extremophilic Archaea on a Mariana forearc serpentinite mud volcano: Ocean Drilling Program Leg 195. *Geochim Geophys Geosy* 4:2009.
- Nielsen SG, Klein F, Kading T, Blusztajn J, Wickham K (2015) Thallium as a tracer of fluid-rock interaction in the shallow Mariana forearc. *Earth Planet Sci Lett* 430:416–426.
- Barnes JD, Sharp ZD, Fischer TP (2008) Chlorine isotope variations across the Izu-Bonin-Mariana arc. *Geology* 36:883–886.
- Alt JC, Shanks WC (2006) Stable isotope compositions of serpentinite seamounts in the Mariana forearc: Serpentinization processes, fluid sources and sulfur metasomatism. *Earth Planet Sci Lett* 242:272–285.
- Kahl WA, Jons N, Bach W, Klein F, Alt JC (2015) Ultramafic clasts from the South Chamorro serpentinite mud volcano reveal a polyphase serpentinization history of the Mariana forearc mantle. *Lithos* 227:1–20.
- McCullom TM (2013) Laboratory simulations of abiotic hydrocarbon formation in Earth's deep subsurface. *Rev Mineral Geochem* 75:467–494.
- Huang WE, Li M, Jarvis RM, Goodacre R, Banwart SA (2010) Shining light on the microbial world the application of Raman microspectroscopy. *Adv Appl Microbiol* 70:153–186.
- Ryugula A, et al. (2013) Raman spectroscopy of proteins: A review. *J Raman Spectrosc* 44:1061–1076.
- Takai K, et al. (2008) Cell proliferation at 122 °C and isotopically heavy CH<sub>4</sub> production by a hyperthermophilic methanogen under high-pressure cultivation. *Proc Natl Acad Sci USA* 105:10949–10954.
- Sharma A, et al. (2002) Microbial activity at gigapascal pressures. *Science* 295:1514–1516.
- Turcotte DL, Schubert G (2014) *Geodynamics* (Cambridge Univ Press, Cambridge, UK).
- Allen DE, Seyfried WE (2004) Serpentinization and heat generation: Constraints from Lost City and Rainbow hydrothermal systems. *Geochim Cosmochim Acta* 68:1347–1354.
- Uyeda S, Horai K (1982) Heat-flow measurements on Deep-Sea Drilling Project Leg-60. *Initial Rep Deep Sea* 60:789–800.
- Kelemen P, Kikawa E, Miller J (2004) Drilling mantle peridotite along the Mid-Atlantic Ridge from 14 to 16 N. *Proceedings of the Ocean Drilling Program, Initial Reports* (Ocean Drilling Program, College Station, TX), pp 1–139.
- Blackwell DD, et al. (1990) Heat-flow in the Oregon Cascade Range and its correlation with regional gravity, curie-point depths, and geology. *J Geophys Res Solid* 95:19475–19493.
- Lewis TJ, et al. (1988) Subduction of the Juan de Fuca Plate: Thermal consequences. *J Geophys Res Solid* 93:15207–15225.
- Peacock SM (2003) *The Subduction Factory*, eds Eiler JM, Abers GA (American Geophysical Union, Washington, DC).
- Syracuse EM, van Keken PE, Abers GA (2010) The global range of subduction zone thermal models. *Phys Earth Planet Inter* 183:73–90.
- Fontaine FJ, Cannat M, Escartin J (2008) Hydrothermal circulation at slow-spreading mid-ocean ridges: The role of along-axis variations in axial lithospheric thickness. *Geology* 36:759–762.
- Hasendever J, et al. (2014) Hybrid shallow on-axis and deep off-axis hydrothermal circulation at fast-spreading ridges. *Nature* 508:508–512.
- Blackman DK, Slagle A, Guerin G, Harding A (2014) Geophysical signatures of past and present hydration within a young oceanic core complex. *Geophys Res Lett* 41:1179–1186.
- Klein F, et al. (2014) Magnetite in seafloor serpentinite—some like it hot. *Geology* 42:135–138.
- Young ED, et al. (2017) The relative abundances of resolved <sup>12</sup>CH<sub>2</sub>D<sub>2</sub> and <sup>13</sup>CH<sub>3</sub>D and mechanisms controlling isotopic bond ordering in abiotic and biotic methane gases. *Geochim Cosmochim Acta* 203:235–264.
- Okland I, Huang S, Thorseth IH, Pedersen RB (2014) Formation of H<sub>2</sub>, CH<sub>4</sub> and N-species during low-temperature experimental alteration of ultramafic rocks. *Chem Geol* 387:22–34.
- McCullom TM (2016) Abiotic methane formation during experimental serpentinization of olivine. *Proc Natl Acad Sci USA* 113:13965–13970.
- Neubeck A, Nguyen DT, Etiope G (2016) Low-temperature dunite hydration: Evaluating CH<sub>4</sub> and H<sub>2</sub> production from H<sub>2</sub>O and CO<sub>2</sub>. *Geofluids* 16:408–420.
- Horita J, Berndt ME (1999) Abiogenic methane formation and isotopic fractionation under hydrothermal conditions. *Science* 285:1055–1057.
- Astruc D, Lu F, Aranzas JR (2005) Nanoparticles as recyclable catalysts: The frontier between homogeneous and heterogeneous catalysis. *Angew Chem Int Ed Engl* 44:7852–7872.
- Kelemen PB, Manning CE (2015) Reevaluating carbon fluxes in subduction zones, what goes down, mostly comes up. *Proc Natl Acad Sci USA* 112:E3997–E4006.
- Busigny V, Cartigny P, Philippot P, Ader M, Javoy M (2003) Massive recycling of nitrogen and other fluid-mobile elements (K, Rb, Cs, H) in a cold slab environment: Evidence from HP to UHP oceanic metasediments of the Schistes Lustrés nappe (western Alps, Europe). *Earth Planet Sci Lett* 215:27–42.
- Sadofsky SJ, Bebout GE (2003) Record of forearc devolatilization in low-T, high-P/T metasedimentary suites: Significance for models of convergent margin chemical cycling. *Geochim Geophys Geosy* 4:9003.
- Sadofsky SJ, Bebout GE (2004) Nitrogen geochemistry of subducting sediments: New results from the Izu-Bonin-Mariana margin and insights regarding global nitrogen subduction. *Geochim Geophys Geosy* 5:Q03115.
- Mikhail S, Sverjensky DA (2014) Nitrogen speciation in upper mantle fluids and the origin of Earth's nitrogen-rich atmosphere. *Nat Geosci* 7:816–819.
- Sverjensky DA, Harrison B, Azzolini D (2014) Water in the deep Earth: The dielectric constant and the solubilities of quartz and corundum to 60 kbar and 1200 °C. *Geochim Cosmochim Acta* 129:125–145.
- Pons ML, et al. (2011) Early Archean serpentinite mud volcanoes at Isua, Greenland, as a niche for early life. *Proc Natl Acad Sci USA* 108:17639–17643.
- Turner S, Rushmer T, Reagan M, Moyer JF (2014) Heading down early on? Start of subduction on Earth. *Geology* 42:139–142.
- Tera F, Papanastassiou DA, Wasserburg GJ (1974) Isotopic evidence for a terminal lunar cataclysm. *Earth Planet Sci Lett* 22:1–21.
- Van Der Meer DG, et al. (2014) Plate tectonic controls on atmospheric CO<sub>2</sub> levels since the Triassic. *Proc Natl Acad Sci USA* 111:4380–4385.
- Hart DJ, Hammon WS, III (2002) Measurement of hydraulic conductivity and specific storage using the shipboard Manheim squeezer. *Proceedings of the Ocean Drilling Program, Initial Reports, 195* (Ocean Drilling Program, College Station, TX), pp 1–15.
- Hernandez B, Coic YM, Pfluger F, Kruglik SG, Ghomi M (2016) All characteristic Raman markers of tyrosine and tyrosinate originate from phenol ring fundamental vibrations. *J Raman Spectrosc* 47:210–220.
- Petriglieri JR, et al. (2015) Micro-Raman mapping of the polymorphs of serpentine. *J Raman Spectrosc* 46:953–958.
- Klein F, Bach W (2009) Fe-Ni-Co-O-S phase relations in peridotite-seawater interactions. *J Petrol* 50:37–59.